Energy & Environmental Science

RSC Publishing

PAPER

View Article Online
View Journal | View Issue

New materials based on a layered sodium titanate for dual electrochemical Na and Li intercalation systems†

Cite this: *Energy Environ. Sci.*, 2013, **6**, 2538

Mona Shirpour,* Jordi Cabana and Marca Doeff

The electrochemical properties of materials derived from $NaTi_3O_6(OH)\cdot 2H_2O$ have been investigated for the first time. The parent compound has a corrugated layered structure consisting of $\{Ti_6O_{14}\}^{4-}$ units with hydrated sodium cations and protons in the interlayer spaces. Upon heating to 600 °C, water is removed irreversibly, the interlayer distances become smaller, and connecting bonds between the octahedral layers form. It was found that this material can reversibly intercalate both lithium and sodium. The initial specific discharge capacities, as measured in half-cells, varied with the state of hydration and the nature of the counter electrode (Na or Li). The electrochemical potential showed a non-linear sloping dependence with degree of intercalation, indicative of a solid-solution mechanism of intercalation. The process was centered at a low average potential of about 0.3 V *vs.* Na or Li, the lowest ever reported for titanate-based Li hosts. The higher density and potential for higher rate capability of this compound, in comparison to carbonaceous materials with similar voltage and reversible capacities, make a compelling case for its development as an anode material, for both lithium and sodium ion batteries.

Received 26th March 2013
Accepted 30th May 2013

DOI: 10.1039/c3ee41037d

www.rsc.org/ees

Broader context

Despite the technological success of lithium ion batteries in small electronics applications, efforts continue to be directed at enabling them to break through the existing barriers to widespread adoption in applications such as electric drive vehicles. Recent attention has been diverted to sodium ion systems due to the attractive cost and abundance features of the raw materials. Finding and designing materials capable of reversibly storing large amounts of electrochemical energy is at the core of technological breakthroughs. While systems based on alloy or conversion reactions lead to huge storage capacities, materials that react with an alkali metal through intercalation reactions are ultimately favored because they require smaller atomic scale rearrangements in comparison, resulting in more durable devices. At the negative electrode, emphasis has been placed on carbonaceous materials. Ti-containing oxides are denser and have higher rate capability than graphite or hard carbons, but they typically show lower capacities and higher voltages of operation, both of which lower energy density. Herein we present results on a new layered titanate that is capable of reversibly intercalating both Li and Na at very low voltages and shows the potential for large storage capacities. Its properties provide insight into the frontiers of electrochemical ion intercalation as it applies to energy storage technologies.

Introduction

Concerns over the long term environmental and economic effects of burning fossil fuels to power our highly technological society have driven scientists, engineers and policymakers to aim for a new infrastructure paradigm based on renewable energy sources that spans from mobility to manufacturing. Energy storage is at the core of this shift through electric drive vehicles and as part of an electrical grid that can respond to the fluctuations that are inherent to wind or sun power. Lithium ion batteries, critical in the advent of our wireless society, have already been commercialized in several hybrid and fully electric cars.[1] However, their success has been limited due to their high cost on a dollars per kilowatt hour basis. Recently, researchers have turned their attention to Na-based technologies because of the higher availability and potential for lower cost of raw materials.[2,3] At the core of enabling these technologies for such large scale applications is the need for active materials that are able to store large amounts of electrochemical energy in a highly reversible and safe manner.

The amount of energy that an active material can store is directly proportional to the moles of Li or Na that it can accept or deliver (*i.e.*, specific capacity) and the voltage at which these redox reactions take place, which is, in turn, dependent on the mechanism. At the negative electrode (anode hereafter), using the elemental alkali metals would be highly desirable, but is ultimately hampered by the inability to strip and plate these metals in a safe and reversible manner, in the case of lithium, and by general safety concerns due to the high reactivity and low melting point of sodium. Alternatively, materials that react with an alkali metal through conversion[4] and alloying[5] mechanisms are intensely investigated for their very high specific capacity and, in some cases, low operating potential. However, they

Environmental Energy Technologies Division, Lawrence Berkeley National Laboratory, University of California, Berkeley, CA 94720, USA. E-mail: MShirpour@lbl.gov

† Electronic supplementary information (ESI) available. See DOI: 10.1039/c3ee41037d

achieve such metrics at the expense of a severe atomic-level reorganization of the structure and huge volume changes that ultimately compromise durability and, subsequently, render them impractical. Alkali metals can also be introduced into a material through topotactic reactions based on intercalation.[6] These reactions involve more subtle structural changes than alloying or conversion reactions, and are thus more likely to lead to long-term stability in devices. Graphite is the anode of choice in commercial Li-ion devices, whereas hard carbons are the leading contenders for future Na-ion technologies.[7,8] This choice is driven by the fact that they show the best combination of high capacity (300+ mA h g^{-1}), durability, and a voltage of operation close to the alkali metal electrodes. However, improvements are sought in their power density, particularly since overpotentials due to ohmic losses in the electrode can lead to hazardous metal plating. The quest for alternatives that can compete with carbonaceous materials pushes the boundaries of our fundamental knowledge of the limits of intercalation reactions as applied to electrochemical energy storage.

Ti-based oxides are an attractive alternative to carbon because they are denser and do not impose a cost penalty. Virtually all TiO_2 polymorphs and a variety of $A_xTiO_{2+x/2}$ (where A = Li, Na) compounds have been extensively studied for applications as Li-ion battery anodes,[9,10] and recent reports exist of their properties as Na^+ ion hosts.[11–13] A broad inspection of the literature reveals that they have the potential for high specific capacities (more than 300 mA h g^{-1}) and extremely high power capability.[9,10] While Li intercalation has only been found to occur at potentials above 1.0 V *vs.* Li^+/Li^0,[9,14] introducing a considerable energy density penalty, Na can be inserted into $Na_2Ti_3O_7$ at ~0.3 V *vs.* Na^+/Na^0 (~0.6 V *vs.* Li^+/Li^0).[15,16] The electrochemical potential at which Na intercalates into a given host is predicted to be lower than for Li,[17] but such inherent differences were found to be between 0.18 and 0.57 V, suggesting that materials able to intercalate Li below 1.0 V *vs.* Li^+/Li^0 should exist. In turn, the challenge for Ti-based oxides proposed as Na-ion anodes[12,15,16,18] is to achieve the sustained cycling at high specific capacity that is now commonplace in Li-ion counterparts.[9,10] For instance, the capacity retention of $Na_2Ti_3O_7$ appears to vary with the cycling rate, particle size and cut-off voltage used.[16] The large dependence of these metrics on the intercalant indicates that they may not be inherent limitations, but the result of insufficient material screening and electrode engineering.

In many ternary alkali titanates, TiO_6 octahedra share corners and/or edges to form two-dimensional structures. The titanate layers are negatively charged, and positively charged species such as alkali metal cations (Li^+, Na^+, K^+, Rb^+, Cs^+) or protons (H^+) are located between the galleries. The nature of these intercalated cations, the synthesis conditions (*i.e.*, temperature, humidity), structure, and surface properties of the octahedral layers (*i.e.*, thickness of the layers, length of the bonds, presence of water and/or protons) tune the interlayer distance and properties of the layered titanate.[19] The versatility of the structural properties makes these materials ideal for a number of applications including ion-exchange, nuclear waste clean-up, and photocatalysis.[20–22]

In this work, we report a new layered titanate phase, derived from the $NaTi_3O_6(OH)\cdot 2H_2O$ structure, that is capable of reversibly intercalating both Li and Na at very low potentials. The parent phase is, in fact, structurally identical to "sodium nonatitanate",[20–22] whose composition varies over the range $Na_{3+x}Ti_9O_{21-\delta}\cdot nH_2O$ (x = 0.8–2.5, δ = 0.2–1.1, n = 6–10) depending on the synthesis conditions.[22] Sodium nonatitanates have found extensive use in the nuclear waste clean-up industry due to their good ion exchange properties. Capacities as high as 300 mA h g^{-1} are predicted for the dehydrated version of $NaTi_3O_6(OH)\cdot 2H_2O$, based on reduction of all of the Ti^{4+} ions to Ti^{3+}. In this publication, we describe the structural changes during dehydration and report the results obtained with both the pristine and dehydrated materials in lithium and sodium half-cell configurations for the first time.

Experimental

$NaTi_3O_6(OH)\cdot 2H_2O$, also known as sodium nonatitanate (and designated NNT hereafter), was synthesized hydrothermally as previously described in the literature.[22] Deionized water (5 mL) was first added to a 50 wt% NaOH solution (7.8 g, Sigma-Aldrich). Then titanium isopropoxide (6.25 g, purity 97%, Aldrich) was added rapidly to the solution while stirring. The white gel that formed in the beaker was mixed for about 10 min and then transferred to a pressure vessel with a 30 mL size Teflon lining for hydrothermal treatment. A heat treatment performed at 200 °C for 20 hours resulted in the highest crystallinity and the lowest amount of $Na_3(CO_3)(HCO_3)\cdot 2H_2O$ (trona) impurity phase in the final composition. The resulting substance was filtered, washed and dried under vacuum at 120 °C for 12 h.

$Na_2Ti_6O_{13}$ and $Na_2Ti_3O_7$ were synthesized by solid-state reactions using stoichiometric amounts of TiO_2 (anatase, purity 99.7%, <25 nm, Sigma-Aldrich) and Na_2CO_3 (purity 99.95+%, Aldrich). The mixtures were calcined at 800 °C for 20 h, followed by grinding, mixing, pelletizing, and a second calcination at 800 °C for 20 h.

X-ray diffraction (XRD) patterns were obtained with a Philips PW3040 X'Pert Pro Diffractometer using a Cu Kα (λ = 1.54056 Å) source operated with a 45 keV X-ray tube voltage, and equipped with an X'celerator detector. Lattice parameters were determined by profile matching with constant scale factor (LeBail fit) using the WinPLOTR/Fullprof suite.[23,24] A high-temperature chamber (Anton Paar HTK 1200N) was used to observe the dependence of the XRD patterns with temperature. The chamber was heated at a rate of 20 °C min^{-1} and scans were obtained after keeping the sample for 1 hour at each temperature. Scanning electron microscopy (SEM) images were obtained using a JEOL JSM-7500F field-emission microscope. Energy dispersive X-ray spectroscopy (EDS) data were collected using a Noran system S1X (Thermo Electron Corporation, model 6714A01SUS-SN) probe attached to the scanning electron microscope. $Na_2Ti_3O_7$ was used as a reference to calibrate the EDS for quantitative elemental analysis of the NNT samples.

Thermogravimetric analysis (TGA) was performed with a SDT Q600 instrument under argon (gas flow 20 mL min^{-1}), using a

heating rate of 10 °C min^{-1}. Raman spectra were collected with a Spex 1877 0.6m Triple Spectrometer equipped with a Princeton Instruments CCD detector and a Lexel 95 Ar^+ ion laser operating at 488 nm and 300 mW. Fourier transform infrared (FTIR) spectra were recorded in the range 400 to 4000 cm^{-1} using a Thermo Nicolet 6700 FTIR spectrometer. The powder samples were dispersed in KBr pellets for measurements in transmission mode under flowing nitrogen gas.

The electrochemical properties of the compounds were evaluated in two-electrode 2032 coin cells containing metallic sodium or lithium as the counter electrode. Sodium disks were made by extruding dry sodium sticks (Sigma-Aldrich) into thin foils and cutting to size. Commercial lithium foils (Alfa Aesar) were used as anodes in the lithium cells. Composite working electrodes were prepared by making a slurry of 70 wt% of sodium titanate, 25 wt% acetylene black (Denka, 50% compressed), and 5 wt% polyvinylidene difluoride (PVDF) (99.5+%, Aldrich) binder in *N*-methyl-2-pyrrolidinone (NMP). The active material and the acetylene black were first mixed for 2 hours at 300 rpm in a planetary mill. The slurry was cast onto carbon coated aluminum foil (Exopack Advanced Coatings; http://www.exopackadvancedcoatings.com/2010/02/conductives-current-collector/) or on copper foil (Pred Materials) for sodium (Sigma-Aldrich) and lithium half-cells, respectively. The electrodes were dried first in air and then under vacuum at 120 °C for 12 h before being cut to size and weighed. The typical loading and thickness were 5 mg cm^{-2} and 60 μm, respectively. The electrolyte used for sodium cells was a solution of 1 M $NaPF_6$ (Sigma-Aldrich) in ethylene carbonate–dimethylene carbonate (EC : DMC) 3 : 7 mol (from Novolyte Technologies) made in-house, whereas commercially available 1 M $LiPF_6$ in EC–DMC 1 : 2 (Novolyte Technologies) was employed in lithium half-cells. Celgard 3401 separators were used in both cases. Galvanostatic cycling experiments and electrochemical impedance spectroscopy (EIS) at room temperature were carried out with a Bio-logic VMP3 potentiostat/galvanostat. The impedance spectra were obtained in the frequency range of 100 kHz to 50 mHz.

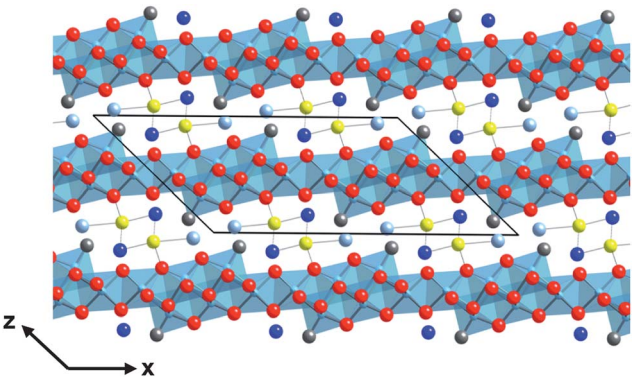

Fig. 1 Crystal structure of $NaTi_3O_6(OH)\cdot 2H_2O$ created with CrystalMaker software. TiO_6 octahedra are in blue, yellow spheres are Na^+ ions, red spheres are O^{2-} ions, dark and light blue spheres are H_2O groups coordinated to Na^+, and grey spheres are OH^- groups connected to Ti^{4+}.

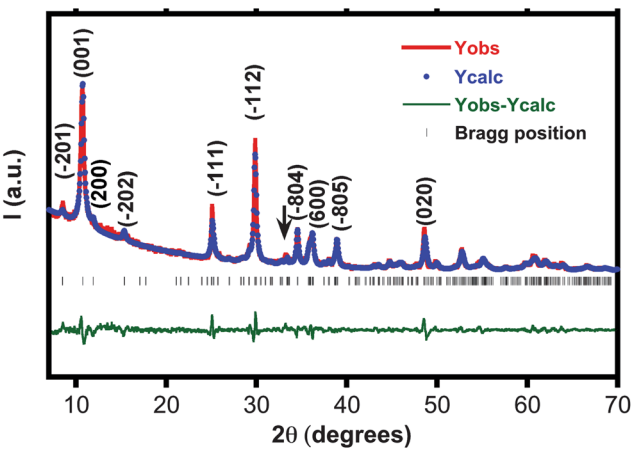

Fig. 2 Experimental XRD pattern (red line) of the as-made sodium titanate sample and the calculated pattern (blue dots) from the profile matching method using WinPLOTR/Fullprof suite. The difference profile is given at the bottom (green line). Bragg positions are indicated by the vertical markers. The arrow corresponds to the $Na_3(CO_3)(HCO_3)\cdot 2H_2O$ (trona) phase impurity.

Results and discussion

The structure of $NaTi_3O_6(OH)\cdot 2H_2O$ (NNT) consists of edge- and corner-sharing TiO_6 octahedra that form corrugated layers of $\{Ti_6O_{14}\}^{4-}$ units, between which hydrated Na^+ cations and protons (H^+) are located (Fig. 1).[25] Each Na^+ is coordinated to three water molecules, and H atoms are located on the least coordinated oxygen atoms at the steps. The structure bears some similarities to $Na_2Ti_3O_7$,[26] which has a stepped layered structure with each unit consisting of three edge-sharing octahedra, $\{Ti_3O_7\}^{2-}$, linked by corners. The $NaTi_3O_6(OH)\cdot 2H_2O$ structure is more open due to the thicker octahedral layers and the presence of interlayer water molecules, consistent with its good ion exchange properties. Fig. 2 shows the indexed experimental XRD pattern of the as-made material. The obtained lattice parameters (Table 1) are in good agreement with previously reported values.[25] The product of the hydrothermal reaction also contained a small amount (estimated at 1–2 vol%) of $Na_3(CO_3)(HCO_3)\cdot 2H_2O$ (trona); a reflection belonging to this phase is marked with an arrow in the figure. A Ti : Na ratio of 2 was found by EDS/SEM, similar to previous reports,[25] but lower than the expected value of 3 for $NaTi_3O_6(OH)\cdot 2H_2O$. The deviations can be ascribed to the presence of the trona impurity and the possibility of Na^+/H^+ exchange during the manipulation of the compound. This ratio has been shown to vary with synthesis and washing procedures, as well as environmental conditions such as humidity and temperature during storage.[22]

Table 1 Structural parameters for the as-made NNT obtained by profile matching using the space group *C*2/*m* (Rwp = 9.1)

Parameter	Refined values	Reported values[25]
a (Å)	21.50(9)	21.53(8)
b (Å)	3.74(1)	3.79(2)
c (Å)	11.88(2)	11.92(8)
β (°)	136.13(7)	136.3(5)

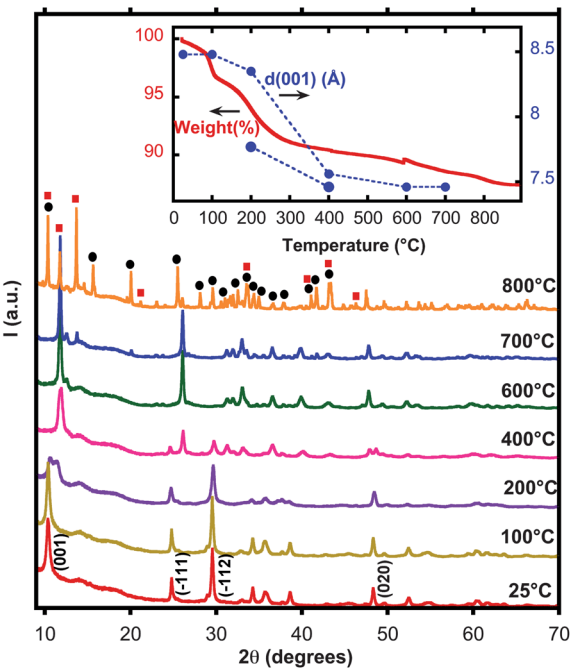

Fig. 3 *In situ* XRD patterns of the as-made NNT sample as a function of temperature. Circles: $Na_2Ti_3O_7$, squares: $Na_2Ti_6O_{13}$. Sample weight loss from TGA experiments and $d_{(001)}$-spacings calculated from the XRD patterns are shown in the inset. See the text for details.

Comparison of the TGA data and XRD patterns collected upon heating the sample reveals a gradual and complex structural change and weight loss with temperature (Fig. 3). The initial step below 100 °C can be ascribed to the departure of physisorbed water as no shift was observed in the (001) reflection of NNT. The second step above 150 °C results in the doubling of the (001) reflection, indicative of the appearance of a second layered phase with smaller interlayer spacing (Δd = 8.33–7.33 = 1 Å). This suggests that the new phase has lower interlamellar water content than the pristine compound. It is likely that the apical water molecules, which are not shared between two adjacent sodium ions (light blue atoms in Fig. 1), and which form weaker bonds, are the first to be released, followed by the molecules with stronger bonds (dark blue atoms in Fig. 1).[27] The dehydration causes a sharp drop in the relative intensity of the (−112) reflection at about $2\theta = 29.7°$. In the as-made material, this plane mainly contains the interlamellar water molecules and the sodium atoms connected to them (Fig. S1†). The atom density of this plane is reduced due to the loss of these molecules and the subsequent movement of the sodium ions into new positions, closer to the titanium-containing layers. At 600 °C, the sample is completely dehydrated and consists primarily of one layered phase structurally related to the as-made NNT, as indicated by the single sharp (001) reflection. The total weight loss corresponds to n = 2–2.1 in the formula $NaTi_3O_6(OH)\cdot nH_2O$. When the temperature was raised above 600 °C, there was a slight weight loss (<3 wt%) accompanied by decomposition of the NNT phase to a mixture of $Na_2Ti_6O_{13}$ and $Na_2Ti_3O_7$. Dehydrated NNT samples (NNT annealed at 600 °C for 2 hours) are stable at room temperature

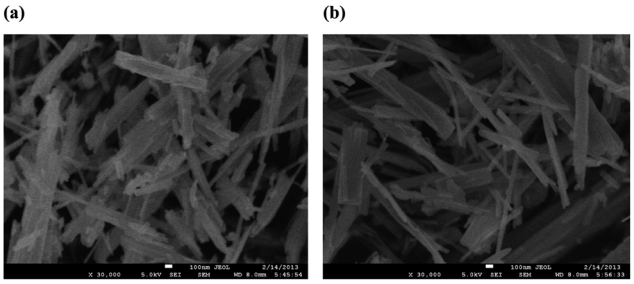

Fig. 4 SEM images of (a) as-made NNT and (b) dehydrated NNT.

and do not take up interlamellar water upon exposure to the atmosphere. The morphology of the as-made NNT was maintained in the dehydrated sample (Fig. 4); both consisted of flat ribbons about 100 nm wide and several microns in length.

Fig. 5 shows the IR spectrum of the as-made and dehydrated NNT. The IR spectra of $Na_2Ti_3O_7$ and $Na_2Ti_6O_{13}$ are also shown for comparison. The NNT samples are clearly different from these compounds. Bending and stretching vibrations of OH groups of weakly bonded, physisorbed water at 1645 and 3430 cm^{-1} were observed in the IR spectrum of the as-made NNT sample.[28,29] These two peaks, although much less intense, were also present in a dehydrated sample stored in air. The bands at 1730 cm^{-1} and 3150 cm^{-1} are associated with the bending and stretching modes of the chemisorbed/interlamellar water molecules.[28,29] In addition, a shoulder at 2900 cm^{-1} was observed in the as-made material, ascribable to the strong interaction between Ti ions and O–H groups. These IR bands were not present in the dehydrated sample, indicating that the interlamellar water was removed and the Ti–OH bonds were modified. Sodium titanates contain Ti–O stretching and bending vibration bands with different intensities in the region 500–1000 cm^{-1},[29,30] the shape and position depending on the specific framework. The peak at 910 cm^{-1} corresponds to Ti–O bonds in TiO_6 octahedra, and the small peak at 974 cm^{-1} is due to the bending vibrations of Ti–OH non-bridging bonds in the as-made sample. The alkali–oxygen vibrations usually give absorption bands at 1440, 1370, 1060, and 880 cm^{-1}.[28] For the

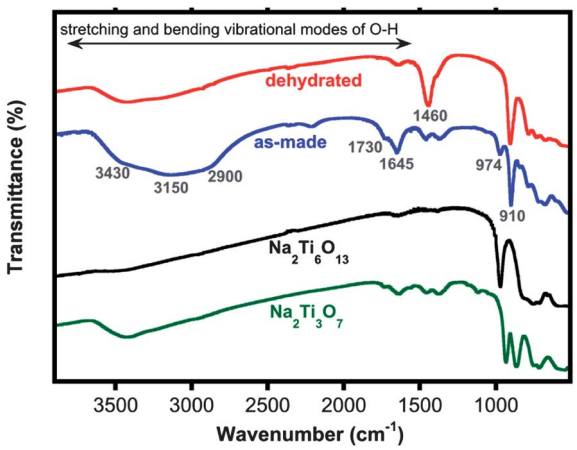

Fig. 5 FTIR spectra of the as-made and the dehydrated samples. $Na_2Ti_3O_7$ and $Na_2Ti_6O_{13}$ FTIR spectra are shown for comparison.

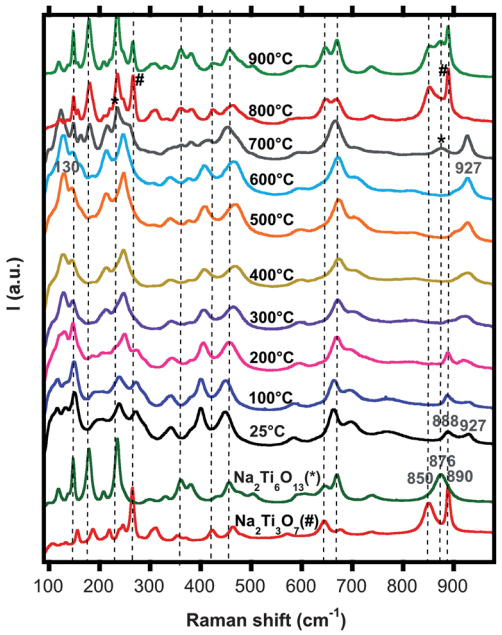

Fig. 6 *Ex situ* Raman spectra for the NNT sample heated between 25 and 900 °C. $Na_2Ti_3O_7$ and $Na_2Ti_6O_{13}$ Raman spectra are shown for comparison.

as-made sample, small peaks can be observed at these frequencies. The sharp peak at 1460 cm^{-1} in the IR spectra of the dehydrated sample is attributable to the formation of new alkali–oxygen (Na–O) bonds.[28,29]

Additional information on the structural changes that accompany the dehydration of NNT was obtained from Raman spectroscopy. Fig. 6 shows Raman spectra collected *ex situ* for samples annealed in the 100 to 900 °C temperature range, and compared with data taken for $Na_2Ti_3O_7$ and $Na_2Ti_6O_{13}$ standards. In previous work on other sodium titanates,[31–33] the bands below 400 cm^{-1} and between 600 and 800 cm^{-1} have been attributed to Na–O bond vibrations and Ti–O stretching vibrations in edge-shared and corner-shared TiO_6 octahedra, respectively. Bands at higher frequencies (800–950 cm^{-1}) have been assigned to short Ti–O bonds of low coordination. The high frequency Raman peak in the spectrum of $Na_2Ti_3O_7$ (890 cm^{-1})[31] corresponds to oxygen atoms coordinated to one titanium atom at a distance of only 1.7 Å (*i.e.*, a step). In contrast, in the tunnel structure of $Na_2Ti_6O_{13}$, every oxygen is bound to at least two Ti atoms at bond distances within the range of 1.9 to 2.3 Å,[34] resulting in a broad peak at 876 cm^{-1} instead.[31] By analogy to the $Na_2Ti_3O_7$ spectrum, the peak at 888 cm^{-1} of the as-made NNT can be assigned to oxygen atoms coordinated to only one Ti; this oxygen is located at the steps where hydroxyl groups are found. These Ti–OH bonds (grey circles in Fig. 1) are 1.9 Å in length.[25] The shortest bonds in the NNT structure, however, correspond to oxygen ions that bond to more than one Ti at lengths of 1.14–1.16 Å. These very short bonds most likely give rise to the Raman peak at the highest frequency, 927 cm^{-1}.

There were significant changes in the Raman bands upon heating (Fig. 6). The spectra of the samples annealed above 700 °C were a combination of those obtained on $Na_2Ti_6O_{13}$ and $Na_2Ti_3O_7$, in agreement with the XRD data (Fig. 3). Above 100 °C, the removal of the structural water groups and condensation of the layered structure causes changes in the bond length and coordination number of the atoms. In samples heated at and above 300 °C, the intensity of the peak at 888 cm^{-1} attributable to the Ti–OH bonds decreased. The peak at 927 cm^{-1} became narrower and more intense, while an overall blueshift is observed in those between 200 and 700 cm^{-1}, indicating decreases in the Ti–O bond distances. In addition, an intense peak appeared at 130 cm^{-1}. While this could be consistent with the formation of Ti–O–Ti bonds as in the tunnel structure $Na_2Ti_6O_{13}$, the overall spectrum is clearly different. Instead, this can be assigned to the formation of a new Ti–O*–Na bond[35] (where O* refers to ions with a single bond to Ti at the steps of the as-made NNT structure) as a result of the displacement of the alkali ions closer to the TiO_6 layers following the desorption of water molecules. It is likely that hydrogen or sodium bridges (*i.e.*, O*–H–O* or O*–Na–O*) subsequently formed pinch points that brought the TiO_6 octahedra closer than in the original compound, resulting in a pseudo-tunnel structure. The advent of the strong peak at 130 cm^{-1} supports the formation of more sodium bridging bonds[35] than hydrogen bridging bonds. The disappearance of the TiOH vibrational modes upon heating is also consistent with formation of hydrogen bridging bonds or ion exchange of Na for H, with thermal decomposition of the trona impurity as the likely source of the extra sodium. A suggested structure for the dehydrated NNT based on these observations is shown in Fig. 7. A more rigorous phase determination using advanced TEM electron diffraction methods is underway and will be presented in a separate publication.

Fig. 8a–d present the first and second cycle voltage profiles of composite electrodes containing as-made or dehydrated NNT in Na and Li half-cells. Initial discharge capacities of about 220–250 mA h g^{-1} were obtained for both electrodes in Na half-cells, with most of the capacity well below 1 V *vs.* Na^+/Na^0. The as-made sample (Fig. 8a) showed poor reversibility, with the specific capacity dropping below 50 mA h g^{-1} by the second cycle. Although the discharge profile was very similar to that of the as-made material (Fig. 8b), the dehydrated sample displayed much better reversibility (125 mA h g^{-1} in the second cycle). When cycled against Li metal, both materials displayed larger than expected initial discharge capacities of about 400 mA h g^{-1}

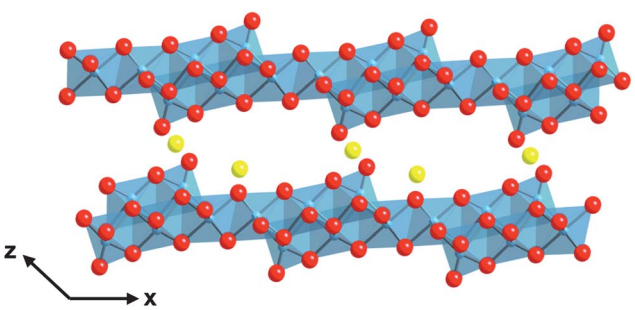

Fig. 7 Suggested structure of the dehydrated NNT phase after removal of the structural water and possible formation of Ti–O–Na or Ti–O–H bonds between layers. The yellow spheres represent Na^+ or H^+.

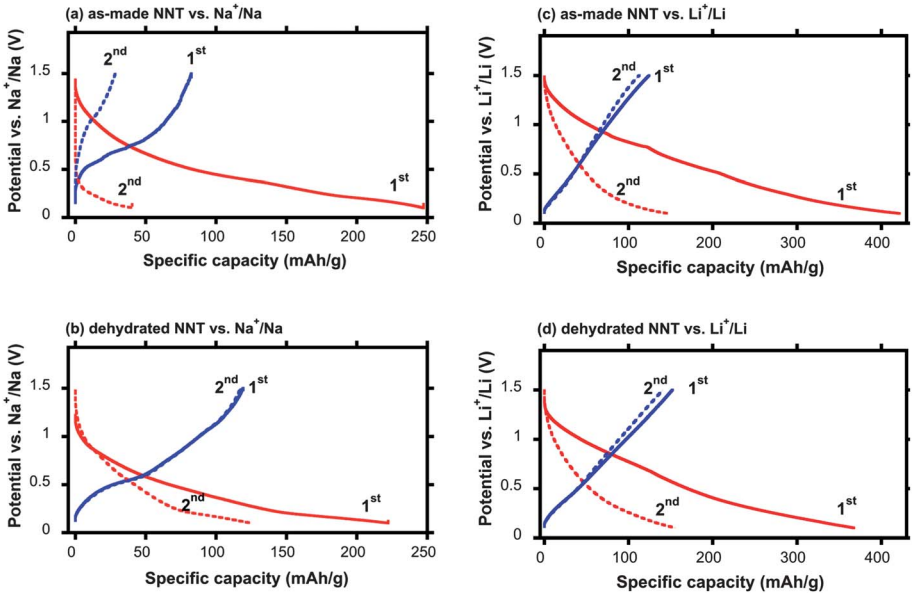

Fig. 8 Voltage *versus* specific capacity profile for the as-made and the dehydrated samples in Na half-cells (a and b) and Li half-cells (c and d) cycled between 1.5 and 0.1 V at 0.15 mA cm^{-2} (30 mA g^{-1}).

(Fig. 8c and d), which dropped to 150 mA h g^{-1} in the second cycle. The reversibility of both the as-made NNT and the dehydrated NNT in lithium cells was similar, in contrast to the behavior in sodium cells. The second cycle discharge capacities of the dehydrated NNT correspond to about 1.3 Na^+ and 1.6 Li^+ ions per formula unit of the active material.

Galvanostatic experiments at lower rates provided insight into the mechanism of electrochemical reaction of the dehydrated NNT electrodes in sodium and lithium cells. Three voltage regions became apparent during discharge in the Na half-cell (Fig. 9a). The corresponding derivative curve (Fig. 9b) exhibited two small and broad peaks at 0.9 V (labeled "I" in the figure) and 0.5 V (region II) *vs.* Na^+/Na^0 and a larger one below 0.2 V (region III). The position of peak I is consistent with the irreversible decomposition of the electrolyte and formation of a solid film at the surface of the electrode.[36] Peak II can be ascribed to the irreversible insertion of sodium into acetylene black based on the results of a blank electrode with no titanate (see Fig. S2†). These two signals became very weak on the first charge and disappeared completely on the second cycle indicating that they correspond to irreversible processes. After the first cycle, the discharge profile consisted of two sloping regions with a break at 0.2 V *vs.* Na^+/Na^0, both of which can be attributed to the insertion of sodium between the titanate layers. These

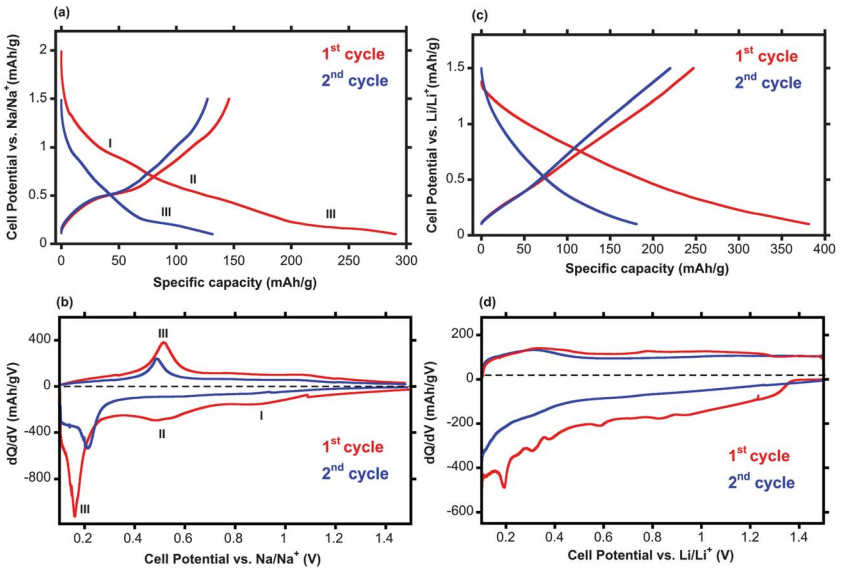

Fig. 9 Voltage profile and derivative curves of the dehydrated sample cycled between 1.5 and 0.1 V at 0.02 mA cm^{-2} (4 mA g^{-1}) in Na half-cells (a and b) and in Li half-cells (c and d).

processes are at least partially reversible over this voltage range. The potentials at which sodium ions insert into NNT are unusually low, as with $Na_2Ti_3O_7$,[15] but the voltage profile is more consistent with a solid solution mechanism rather than one that is two-phase.

The voltage profile and derivative curve of dehydrated NNT in a Li half-cell at low discharge rates are also shown in Fig. 9c and d. Features attributable to SEI formation and insertion of Li into acetylene black are less clearly delineated in the dQ/dV plot of the lithium cell than in the sodium cell; instead one rather broad peak with smaller peaks superimposed on it is observed. This suggests that there are multiple sites for lithium insertion and that they overlap with the SEI formation and irreversible insertion of lithium into the acetylene black.

Fig. 10 depicts the evolution of the capacity values of the Na and Li half-cells shown in Fig. 8 upon extended cycling. For the as-made NNT, the initial Coulombic efficiency was very low in both lithium and sodium half-cells. However, while the capacity of the sodium cell dropped to negligible values by the fifth cycle, it stabilized at above 100 mA h g^{-1} after 20 cycles in the case of lithium. The irreversibility of the as-made NNT in both cases is likely due, at least in part, to electrochemical and chemical processes in the cell associated with free water that may deintercalate from NNT during cycling and reduce to H_2 at the very low potentials reached in the experiment. Side reactions such as irreversible intercalation of lithium or sodium ions into the carbon black additives and reduction of the electrolytic solution to form a solid electrolyte interface also contributed to the irreversibility in the first cycle. However, the much worse behavior of the as-made NNT in sodium cells suggests that additional factors are at play. The larger size of sodium ions compared to lithium may induce larger volume changes during insertion processes, leading to exfoliation or disconnection and isolation of particles and concomitant loss of capacity. In contrast, the cycling behavior of dehydrated NNT was significantly better than that of the as-made material. The Na and Li half-cells sustained capacities above 100 mA h g^{-1} and 120 mA h g^{-1} for 20 cycles, respectively, with larger initial Coulombic efficiencies.

Electrochemical impedance spectra were recorded after each discharge to 0.1 V and each charge to 1.5 V for three types of cells; sodium cells containing the as-made NNT and dehydrated NNT, and lithium cells containing the as-made NNT. The Nyquist plots (Fig. S3†) were fitted using an equivalent circuit with three components (R1, (R2||Q2), and (R3||Q3)). By analogy to Li-ion cells,[36] R1 was assumed to be the ohmic resistance of the electrode, electrolyte, separator, and connections in the cell. The first semicircle at high frequencies (R2) is associated with the reaction layer that forms on the alkali metal anode in contact with the electrolytic solution.[37] These two values (R1 and R2) changed very little for the three types of cells during cycling, after both charging and discharging (Fig. 11). In contrast, the value for the second semicircle (R3) in the spectrum of the as-made NNT electrode in a sodium cell increased 5–10 fold upon cycling, but remained relatively stable for the other two cells. This semicircle has been associated with the conducting properties of the electrode (the ionic/electronic conductivity of the electrode) and/or charge transfer through the electrode–electrolyte interface.[36] Therefore, the significant increase for the as-made NNT/Na cell upon cycling is suggestive of a deterioration of the composite electrode, which could be due to exfoliation or expansion of the layered structure resulting in disconnection of particles and loss of capacity, as posited above.

There are multiple features that make NNT, particularly in its dehydrated form, into a compelling new choice as an

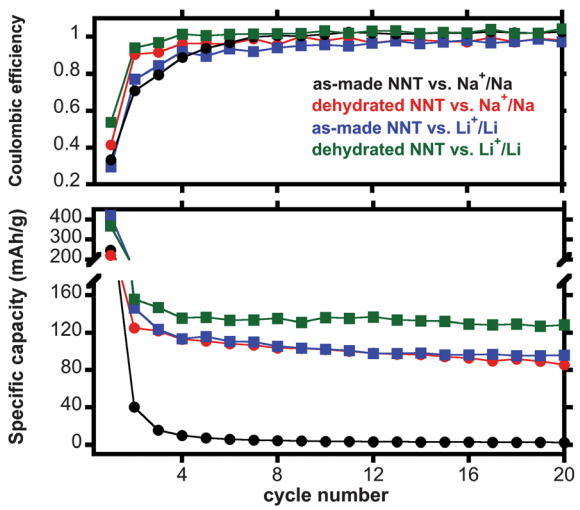

Fig. 10 Specific discharge capacity and Coulombic efficiency as a function of cycle number for the as-made and the dehydrated samples in Na and Li half-cells cycled between 1.5 and 0.1 V at 0.15 mA cm^{-2} (30 mA g^{-1}).

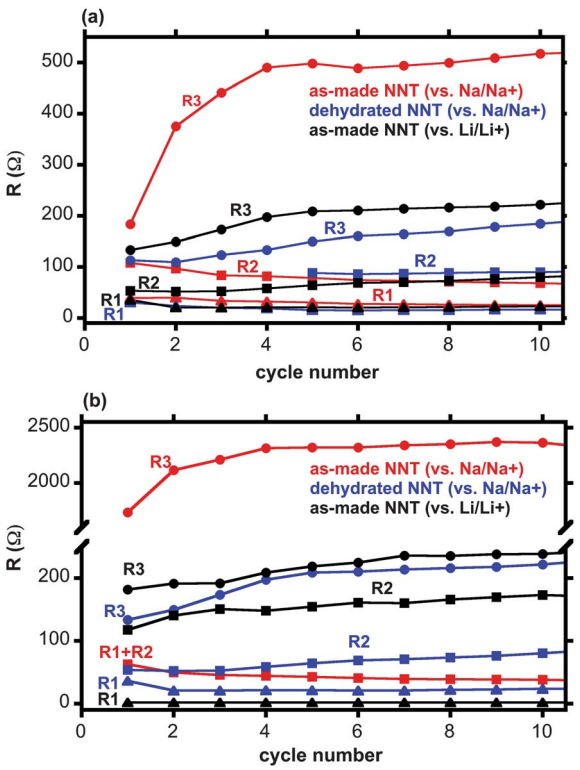

Fig. 11 Resistivity values (R1, R2, R3) extracted from the AC impedance spectra for the as-made and dehydrated NNT in Na half-cells and Li half-cells after (a) discharge to 0.1 V and (b) charge to 1.5 V.

electrode for both Na- and Li-ion batteries. It is remarkable that the voltage at which Li insertion into dehydrated NNT occurs is well below 1.0 V *vs.* Li^+/Li^0. Although Na insertion at low potentials is known, for instance, for $Na_2Ti_3O_7$,[15] such low potentials for lithium reactions normally involve conversion or alloying,[4,5] and have been demonstrated for very few intercalation compounds, such as graphite[38] and $Li_{1+x}V_{1-x}O_2$,[39,40] which both lithiate at ~100 mV *vs.* Li^+/Li^0. It is in part because of this low potential that graphite is the electrode of choice in commercial Li-ion devices. In contrast, all binary and ternary titanium oxides reported in the literature undergo Li intercalation primarily between 1.7 and 1.0 V *vs.* Li^+/Li^0,[9,14,41–43] which limits their utility to devices intended for applications that do not require high energy density. The low potentials are advantageous for anode materials, as they raise both the energy density and specific energy. For example, a sodium ion battery consisting of a Na_2FePO_4F cathode (capacity: 120 mA h g^{-1}, 3.0 V *vs.* Na^+/Na^0)[44] paired with $NaTi_2(PO_4)_3$ (capacity: 120 mA h g^{-1}, 2.0 V *vs.* Na^+/Na^0)[45] would have a theoretical specific energy of about 60 W h kg^{-1}. By pairing the same cathode with a 0.3 V anode of 120 mA h g^{-1} capacity, the theoretical specific energy is increased to 160 W h kg^{-1}. If the full theoretical capacity of 300 mA h g^{-1} for the NNT electrode could be cycled, the system theoretical specific energy would be increased to 230 W h kg^{-1}. Layered sodium titanates also have volumetric advantages compared to anodes based on carbonaceous materials, due to their higher densities (2.5–3.5 g cm^{-3} compared to 1.5–2.25 g cm^{-3}). If the full capacity of the dehydrated NNT could be made to cycle in a lithium ion configuration using an NMC ($LiNi_{1/3}Mn_{1/3}Co_{1/3}O_2$) cathode, the theoretical energy density would rise to 1490 W h L^{-1} from 1400 W h L^{-1} calculated for the same system using a conventional graphite anode (assuming a density of 3.5 g cm^{-3} for the dehydrated NNT compared to 2.25 g cm^{-3} for graphite).

The largely sloping voltage profiles of the NNT electrodes in Na and Li half-cells are indicative of a solid solution mechanism of alkali metal insertion over a wide composition range. Such behavior is in stark contrast with the trends for all other binary and ternary titanium oxides (*e.g.* TiO_2, $Li_xTiO_{2+x/2}$, $Na_2Ti_3O_7$, $Na_2Ti_6O_{13}$) known to accommodate these ions, which show significant compositional domains of first order transitions.[12,15,41–43,46] In terms of the durability of the electrode, this behavior can have a potentially significant beneficial impact because mechanical strain can build up at the phase boundaries that form during the transition between two phases, particularly when anisotropic volume changes exist between them.[47] As a result, materials undergoing solid solution processes are more likely to be mechanically stable during sustained cycling. Therefore, improvements in electrode utilization, which bring the specific capacity closer to the theoretical values, and capacity retention, particularly between the first and second cycles, could be envisaged through judicious electrode and materials engineering. For example, because diffusion of sodium is presumably anisotropic in this layered material, it would help to decrease the length of the ribbons, whose long axes are oriented along the 100 direction.[25] This modification would reduce the risk of over-reduction of particles during discharge, which should improve the reversibility, as well as allow less carbon to be used in the electrode,[48] decreasing one source of the first cycle irreversibility. The use of a carbon additive with lower surface area than that of acetylene black should also help improve efficiencies.[49] The use of SEI forming additives like fluoroethylene carbonate as has been used successfully in a recent publication[50] and optimization of the electrolytic solution should also help reduce the first cycle irreversibility, as would ensuring the effective removal of all protonated species. In particular, it has recently been found that DMC-based electrolytic solutions result in higher coulombic inefficiencies than mixtures of ethylene carbonate (EC) and propylene carbonate (PC) used in dual sodium intercalation systems with carbon anodes.[51] Large volume changes, which may result in particle disconnection and isolation, can be ameliorated by using more compliant binders, as has been done recently for silicon anodes with success.[52–54] Although volume changes associated with intercalation reactions are generally much smaller than those of conversion or alloying reactions, sodium insertion reactions are expected to have a bigger effect on host structures than the corresponding lithium insertion reactions because of the larger size of the former. Because of the significant progress made by the research community in engineering TiO_2 electrode materials so that they can deliver sustained capacities above 200 mA h g^{-1} at very high cycling rates,[46,55–57] it is realistic to expect that room for improvement still exists with NNT by applying the lessons learned in this process. To optimize these electrodes correctly, however, more information is needed about the sodium and lithium insertion processes into NNT electrodes and the volume or structural changes that occur. We are currently carrying out *in situ* XRD and XAS experiments to improve our understanding, as well as exploring the use of other binders; these results will be published in the near future.

Conclusions

The layered structure $NaTi_3O_6(OH)\cdot 2H_2O$, also known as sodium nonatitanate (NNT), and its dehydrated form have been shown, for the first time, to undergo reductive alkali metal intercalation reactions in lithium and sodium half-cells at very low voltages. These low potentials have no precedent in the literature of intercalation hosts for lithium based on titanates. They also indicate that the large apparent voltage shift for electrochemical insertion of Na with respect to Li reported for these materials is not inherent to the nature of the intercalant, thus providing new insight into the fundamentals of these technologically relevant reactions. The high theoretical capacity, low insertion potentials, and solid solution intercalation mechanism of the dehydrated material have important implications for the development of high energy density dual intercalation systems based on either sodium or lithium. They provide a compelling rationale for further development of the dehydrated NNT as an anode material for sodium ion and lithium ion batteries. To this end, several strategies are suggested for improving the reversibility of the intercalation processes of this material in order to realize the full extent of the high energy density.

Acknowledgements

This work was supported by the Laboratory Directed Research and Development Program of Lawrence Berkeley National Laboratory under U.S. Department of Energy Contract DE-AC02-05CH11231.

References

1 C. Wu, *MRS Bull.*, 2010, **35**, 650–651.
2 V. Palomares, P. Serras, I. Villaluenga, K. B. Hueso, J. Carretero-Gonzalez and T. Rojo, *Energy Environ. Sci.*, 2012, **5**, 5884–5901.
3 B. L. Ellis and L. F. Nazar, *Curr. Opin. Solid State Mater. Sci.*, 2012, **16**, 168–177.
4 J. Cabana, L. Monconduit, D. Larcher and M. R. Palacín, *Adv. Mater.*, 2010, **22**, E170–E192.
5 C.-M. Park, J.-H. Kim, H. Kim and H.-J. Sohn, *Chem. Soc. Rev.*, 2010, **39**, 3115–3141.
6 M. S. Whittingham, *Science*, 1976, **192**, 1126–1127.
7 P. Thomas and D. Billaud, *Electrochim. Acta*, 2002, **47**, 3303–3307.
8 D. A. Stevens and J. R. Dahn, *J. Electrochem. Soc.*, 2000, **147**, 1271–1273.
9 Z. Yang, D. Choi, S. Kerisit, K. M. Rosso, D. Wang, J. Zhang, G. Graff and J. Liu, *J. Power Sources*, 2009, **192**, 588–598.
10 D. Deng, M. G. Kim, J. Y. Lee and J. Cho, *Energy Environ. Sci.*, 2009, **2**, 818–837.
11 H. Xiong, M. D. Slater, M. Balasubramanian, C. S. Johnson and T. Rajh, *J. Phys. Chem. Lett.*, 2011, **2**, 2560–2565.
12 N. D. Trinh, O. Crosnier, S. B. Schougaard and T. Brousse, *ECS Trans.*, 2011, **35**, 91–98.
13 Z. Bi, M. P. Paranthaman, P. A. Menchhofer, R. R. Dehoff, C. A. Bridges, M. Chi, B. Guo, X.-G. Sun and S. Dai, *J. Power Sources*, 2013, **222**, 461–466.
14 J. C. Perez-Flores, C. Baehtz, M. Hoelzel, A. Kuhn and F. Garcia-Alvarado, *RSC Adv.*, 2012, **2**, 3530–3540.
15 P. Senguttuvan, G. Rousse, V. Seznec, J.-M. Tarascon and M. Rosa Palacin, *Chem. Mater.*, 2011, **23**, 4109–4111.
16 A. Rudola, K. Saravanan, C. W. Mason and P. Balaya, *J. Mater. Chem. A*, 2013, **1**, 2653–2662.
17 S. P. Ong, V. L. Chevrier, G. Hautier, A. Jain, C. Moore, S. Kim, X. Ma and G. Ceder, *Energy Environ. Sci.*, 2011, **4**, 3680–3688.
18 S. H. Woo, Y. Park, W. Y. Choi, N. S. Choi, S. Nam, B. Park and K. T. Lee, *J. Electrochem. Soc.*, 2012, **159**, A2016–A2023.
19 G. D. Ilyushin, *Crystallogr. Rep.*, 2006, **51**, 715–723.
20 J. Lehto and A. Clearfield, *J. Radioanal. Nucl. Chem. Lett.*, 1987, **118**, 1–13.
21 S. F. Yates and P. Sylvester, *Sep. Sci. Technol.*, 2001, **36**, 867–883.
22 A. Merceille, E. Weinzaepfel, Y. Barre and A. Grandjean, *Adsorption*, 2011, **17**, 967–975.
23 J. Rodriguezcarvajal, *Physica B*, 1993, **192**, 55–69.
24 WinPLOTR software at http://www-llb.cea.fr/fullweb/winplotr/winplotr.htm.
25 I. Andrusenko, E. Mugnaioli, T. E. Gorelik, D. Koll, M. Panthoefer, W. Tremel and U. Kolb, *Acta Crystallogr., Sect. B: Struct. Sci.*, 2011, **67**, 218–225.
26 O. V. Yakubovich and V. V. Kireev, *Crystallogr. Rep.*, 2003, **48**, 24–28.
27 M. F. Iozzi, C. Bisio, T. Regi-Macedo, C. Airoldi, M. Cossi and L. Marchese, *J. Mater. Chem.*, 2009, **19**, 2610–2617.
28 B. V. Janakirama Rao, *J. Am. Ceram. Soc.*, 1964, **47**, 455–463.
29 A. M. Bobrova, I. G. Zhigun, M. I. Bragina and A. A. Fotiev, *Zh. Prikl. Spektrosk.*, 1968, **8**, 96–101.
30 G. W. Peng, S. K. Chen and H. S. Liu, *Appl. Spectrosc.*, 1995, **49**, 1646–1651.
31 C. E. Bamberger and G. M. Begun, *J. Am. Ceram. Soc.*, 1987, **70**, C48–C51.
32 H. M. Kim, F. Miyaji, T. Kokubo and T. Nakamura, *J. Mater. Sci.: Mater. Med.*, 1997, **8**, 341–347.
33 Y. Su, M. L. Balmer and B. C. Bunker, *J. Phys. Chem. B*, 2000, **104**, 8160–8169.
34 Y. Wang, T. Sun, D. Yang, H. Liu, H. Zhang, X. Yao and H. Zhao, *Phys. Chem. Chem. Phys.*, 2012, **14**, 2333–2338.
35 F. Miyaji, T. Yoko, H. Kozuka and S. Sakka, *J. Mater. Sci.*, 1991, **26**, 248–252.
36 M. D. Levi and D. Aurbach, *J. Phys. Chem. B*, 1997, **101**, 4630–4640.
37 E. Peled, D. Golodnitsky and G. Ardel, *J. Electrochem. Soc.*, 1997, **144**, L208–L210.
38 R. Fong, U. Vonsacken and J. R. Dahn, *J. Electrochem. Soc.*, 1990, **137**, 2009–2013.
39 N.-S. Choi, J.-S. Kim, R.-Z. Yin and S.-S. Kim, *Mater. Chem. Phys.*, 2009, **116**, 603–606.
40 A. R. Armstrong, C. Lyness, P. M. Panchmatia, M. S. Islam and P. G. Bruce, *Nat. Mater.*, 2011, **10**, 223–229.
41 B. Zachau-Christiansen, K. West, T. Jacobsen and S. Atlung, *Solid State Ionics*, 1988, **28–30**, 1176–1182.
42 J. Akimoto, K. Chiba, N. Kijima, H. Hayakawa, S. Hayashi, Y. Gotoh and Y. Idemoto, *J. Electrochem. Soc.*, 2011, **158**, A546–A549.
43 K. Chiba, N. Kijima, Y. Takahashi, Y. Idemoto and J. Akimoto, *Solid State Ionics*, 2008, **178**, 1725–1730.
44 Y. Kawabe, N. Yabuuchi, M. Kajiyama, N. Fukuhara, T. Inamasu, R. Okuyama, I. Nakai and S. Komaba, *Electrochem. Commun.*, 2011, **13**, 1225–1228.
45 S. Il Park, I. Gocheva, S. Okada and J.-i. Yamaki, *J. Electrochem. Soc.*, 2011, **158**, A1067–A1070.
46 Y. Ren, Z. Liu, F. Pourpoint, A. R. Armstrong, C. P. Grey and P. G. Bruce, *Angew. Chem., Int. Ed.*, 2012, **51**, 2164–2167.
47 N. Meethong, H. Y. S. Huang, S. A. Speakman, W. C. Carter and Y. M. Chiang, *Adv. Funct. Mater.*, 2007, **17**, 1115–1123.
48 C. Kim, N. S. Norberg, C. T. Alexander, R. Kostecki and J. Cabana, *Adv. Funct. Mater.*, 2012, **23**, 1214–1222.
49 S. Komaba, W. Murata, T. Ishikawa, N. Yabuuchi, T. Ozeki, T. Nakayama, A. Ogata, K. Gotoh and K. Fujiwara, *Adv. Funct. Mater.*, 2011, **21**, 3859–3867.

50 S. Komaba, T. Ishikawa, N. Yabuuchi, W. Murata, A. Ito and Y. Ohsawa, *ACS Appl. Mater. Interfaces*, 2011, **3**, 4165–4168.
51 A. Ponrouch, E. Marchante, M. Courty, J.-M. Tarascon and M. Rosa Palacin, *Energy Environ. Sci.*, 2012, **5**, 8572–8583.
52 N. S. Hochgatterer, M. R. Schweiger, S. Koller, P. R. Raimann, T. Woehrle, C. Wurm and M. Winter, *Electrochem. Solid-State Lett.*, 2008, **11**, A76–A80.
53 U. Kasavajjula, C. Wang and A. J. Appleby, *J. Power Sources*, 2007, **163**, 1003–1039.
54 W. R. Liu, M. H. Yang, H. C. Wu, S. M. Chiao and N. L. Wu, *Electrochem. Solid-State Lett.*, 2005, **8**, A100–A103.
55 Y. S. Hu, L. Kienle, Y. G. Guo and J. Maier, *Adv. Mater.*, 2006, **18**, 1421–1426.
56 D. Wang, D. Choi, J. Li, Z. Yang, Z. Nie, R. Kou, D. Hu, C. Wang, L. V. Saraf, J. Zhang, I. A. Aksay and J. Liu, *ACS Nano*, 2009, **3**, 907–914.
57 J.-Y. Shin, D. Samuelis and J. Maier, *Adv. Funct. Mater.*, 2011, **21**, 3464–3472.